PHYSICAL REVIEW B VOLUME 16, NUMBER 10 15 NOVEMBER 1977

Homogeneous strain response of the Fermi surface of molybdenum*

R. Griessen†
Department of Physics, University of Toronto, Toronto, Canada

M. J. G. Lee
Department of Physics and Scarborough College, University of Toronto, Toronto, Canada

D. J. Stanley‡
Department of Physics, University of Toronto, Toronto, Canada

(Received 25 May 1976)

The response of the Fermi surface of a cubic transition metal to homogeneous uniaxial deformation of the lattice is investigated in detail both experimentally and theoretically for the first time. The uniaxial stress dependence of several cross sections of the Fermi surface of molybdenum is measured by the combined oscillatory magnetostriction and torque method, and the results are analyzed to yield separately the dependence on tetragonal shear and isotropic dilation. The Korringa-Kohn-Rostoker method of band-structure calculation is extended to include the effects of uniaxial strain. The experimental results are compared with those calculated from a phase-shift model derived from measured Fermi-surface cross sections, and the volume dependence of the phase shifts is determined from the dilation data. Quantitative predictions of the angular shear dependence of the areas of principal orbits on the Fermi surface of molybdenum are made on the basis of the phase-shift model.

I. INTRODUCTION

The shape of the Fermi surface of molybdenum has been established in great detail by experimental investigations of magnetoresistance,[1,2] magnetoacoustic effect,[3] radio-frequency size effect,[4,5] and de Haas–van Alphen effect.[6,7] The recent de Haas–van Alphen measurements of Hoekstra and Stanford[7] established the de Haas–van Alphen frequencies of various extremal orbits with an experimental uncertainty of typically 0.5%. These authors also developed inversion procedures to estimate certain caliper dimensions of the Fermi surface. Ketterson, Koelling, Shaw, and Windmiller[8] succeeded in fitting the experimental data to within experimental uncertainty by a model constant-energy surface derived from the relativistic Korringa-Kohn-Rostoker (KKR) method of band-structure calculation,[9] adapted to allow for departures from sphericity in the potential within the muffin-tin spheres. They found that the Fermi-surface area data can be accurately parametrized in terms of the phase shifts $\eta_{\Gamma_6^+,0,1/2}$, $\eta_{\Gamma_6^-,1,1/2}$, $\eta_{\Gamma_8^-,1,3/2}$, $\eta_{\Gamma_8^+,2,3/2}$, $\eta_{\Gamma_7^+,2,5/2}$, and $\eta_{\Gamma_8^+,2,5/2}$, associated with the irreducible representations of the cubic group, together with a parameter α which represents the coupling between the two Γ_8^+ representations that is brought about by the cubic crystal field. The limit $\alpha = 0$ corresponds to a parametrization that is diagonal in the angular momentum representation. Ketterson *et al.* obtained the best fit to the molybdenum data with a value of α that differs significantly from zero. This implies that departure from the spherical form of the potential in the muffin-tin spheres is an important physical effect, which must be taken into account if precise agreement with the experimental areas (especially of the neck and ball orbits) is to be obtained. From their model surface they were able to determine the best values of the cubic phase shifts and α, and also to extract the radii of various sheets of the Fermi surface of molybdenum with high precision.

On the basis of this work, a picture emerges of the shape of the Fermi surface of molybdenum that is entirely consistent with the magnetoacoustic effect, radio-frequency size effect, and de Haas–van Alphen effect data. The phase-shift parameters determined from the Fermi-surface data completely characterize the scattering of conduction electrons at the Fermi surface of molybdenum. Thus the geometrical shape of the Fermi surface of molybdenum is now completely understood, both in geometrical terms and in microscopic terms.

The purpose of the present work is to explore further the electronic structure of molybdenum at the Fermi energy by determining the way the Fermi surface is deformed when a homogeneous strain is applied to a single crystal of the metal, and to interpret the experimental data in microscopic terms. The first measurement of the uniaxial stress dependence of the Fermi surface of the transition metal was carried out by Posternak *et al.*[10] Molybdenum was selected for this investigation because its Fermi surface is relatively

simple, and typical of several important transition metals. Only the electron lenses were investigated, however, because the available magnetic field was restricted to 2.2 T.

In this paper we shall consider the response of the Fermi surface to uniaxial stress along the [001] direction of the crystal lattice, and investigate especially effects which are related to changes of crystal symmetry. The present measurements are carried out in fields up to 10.7 T, which makes it possible to extend the measurements to principal orbits on all sheets of the Fermi surface. From separate measurements of the uniaxial stress dependence $d\ln A/d\sigma$ of extremal cross sections of the Fermi surfaces for magnetic fields along the [100], [010], and [001] directions, the strain response $d\ln A/d\epsilon$ can be determined using the elastic constants. This information determines completely the response of the orbit to any orthorhombic deformation.

The strain responses $d\ln A/d\epsilon$ can be discussed most transparently by defining three volume-conserving tetragonal shears γ_i along the cube axes of the conventional unit cell of volume Ω. Then the response to any orthorhombic deformation can be expressed in terms of the three shear responses $d\ln A/d\gamma_i$, together with the dilation response $d\ln A/d\ln\Omega$. The tetragonal shears involve no volume change. Therefore, no change in scalar parameters such as the Fermi energy or the phase shifts of the lattice potential can be associated with an infinitesimal tetragonal shear. In our model, the quantities $d\ln A/d\gamma_i$ are fully determined by the geometrical form of the lattice distortion. So if the phase shifts can be determined from an analysis of the cross-sectional areas of the undistorted Fermi surface, an appropriate calculation involving no additional parameters will yield the tetragonal shear response. In practice, fits to Fermi-surface areas are sometimes rather insensitive to a particular phase shift or spin-orbit parameter. In such cases, the tetragonal shear response may yield information complementary to that which can be deduced from the shape of the Fermi surface of the unstrained metal.

Consider now the dilation response. From the experimental point of view, the data complement those that have been obtained by direct measurement of response to hydrostatic pressure.[11] That good agreement is found between the two sets of experimental data attests to the accuracy of the data. In our model a hydrostatic strain will be accompanied by changes in both the Fermi energy and the phase shifts. So interpretation of the experimental data can yield estimates of the volume derivatives of the phase shifts and of the Fermi energy. Because these otherwise unknown parameters are involved, however, hydrostatic strain response proves to be of little help in improving the band structure of the unstrained metal at the Fermi energy.

The class of strains discussed above, corresponding to extensions along the cube axes of the conventional unit cell, does not include all possible deformations to which a crystal can be subjected. A further class of strains, relative rotations of the cube axes, completes the set. These volume-conserving strains will be termed "angular shears." Although no measurements of angular-shear response of extremal orbits on the Fermi surface of molybdenum are reported in this paper, we present results of calculations based on a model similar to the one employed to calculate the tetragonal shear response. In our model the response to angular shear is fully determined by the geometrical nature of the deformation. As in the case of tetragonal shear, experimental measurements of angular shear will provide a test of our calculation, and may contribute to an improved characterization of the band structure at the Fermi energy.

The tetragonal- and angular-shear responses are, however, more than a means of verifying or improving Fermi-surface models. They are closely related to the deformation parameters that govern such physical properties of a metal as the electron-phonon interaction and the attenuation of acoustic waves.[12] Thus, to construct a model of tetragonal- and angular-shear response and dilation response based on the band structure of the unstrained metal is to take an important step towards a quantitative theory of acoustic-wave propagation in metals. For this reason we shall be concerned not only to understand the experimental data in microscopic terms, but also to develop a model by which the experimental data can be interpolated to yield the response to a given deformation point by point over the Fermi surface.

Subsequent sections of this paper are arranged as follows. In Sec. II, the experimental technique is described and the measurements of the uniaxial stress responses for various symmetry orbits on the Fermi surface of molybdenum are presented. In Sec. III, the method of calculation of the uniaxial strain responses is described. The results for tetragonal-shear response are compared with the experimental data, and the volume dependences of the phase shifts are determined from the hydrostatic strain response. In Sec. IV, our calculation of the response of the Fermi surface of molybdenum to angular shear is presented. Finally, in Sec. V, the results and conclusions of this work are discussed.

II. MEASUREMENT OF STRAIN RESPONSE

The uniaxial stress dependence of Fermi-surface cross sections can be measured by the combined oscillatory magnetostriction[13] and torque method as discussed in detail by Griessen and Sorbello.[14] For an extremal orbit of area A, the stress derivative $d\ln A/d\sigma$ is determined from the equation

$$\frac{d\ln A}{d\sigma} = -\frac{\Delta L/L}{\tau}\frac{d\ln A}{d\Phi}, \tag{1}$$

where $\Delta L/L$ is the amplitude of the oscillatory length changes in a given magnetic field, and τ is the amplitude of the de Haas–van Alphen torque per unit volume. The factor $d\ln A/d\Phi$ in Eq. (1) is determined by measuring the angular dependence of the de Haas–van Alphen frequency of the extremal orbit. The sign of $d\ln A/d\sigma$ is determined by the relative phase between the magnetostriction oscillations and the torque oscillations, and therefore both quantities $\Delta L/L$ and τ must be measured simultaneously. The measurements were carried out with the dilatorquemeter shown in Fig. 1, which is similar to that described by Posternak *et al.*[10] It consists of three main parts: an armature (A_i) mounted on the cryostat, a torquemeter (T_i), and a dilatometer (D_i).

The torquemeter is a modified version of that described in Ref. 10, and fits into the bore of a 10.7 T superconducting solenoid. The spherical part T_1 can be rotated about an axis perpendicular to the field by means of the gears A_2 and the rod A_3. The moveable part T_2 is supported by a double crossed-springs system T_3 which allows rotation to occur without friction. The capacitance measured between the two capacitor plates T_4 is used to detect any relative movement of the moveable part T_2. The torque generated by passing a known current through the coil T_5 is used for an absolute calibration of the capacitance changes. No feedback system is required in our torquemeter because the great sensitivity of the capacitance technique makes it possible to detect very small displacements and thus to use rather rigid suspension springs.

A cross section of the dilatometer also is shown in Fig. 1. The sample D_1 is glued on a slightly conical piece of polycrystalline molybdenum to avoid any thermal stress during cooling down to liquid-helium temperatures. The conical piece D_2 is insulated from the body of the cell D_3. The upper face of the sample acts as one of the capacitor plates. The other capacitor plate D_4 is insulated and glued into the end piece D_5, which is bolted to the dilatometer with a spacer of thickness such that, at low temperatures, the gap between the capacitor plate and the sample is typically 0.01 mm.

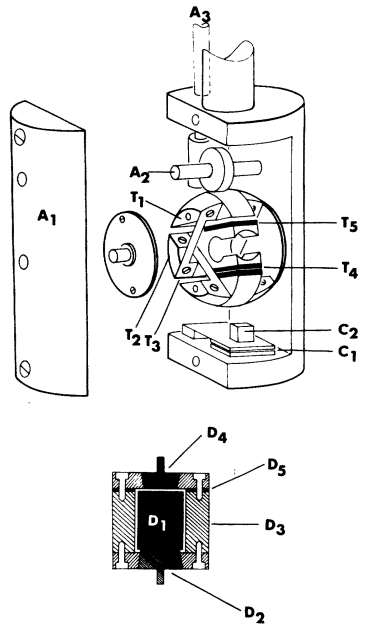

FIG. 1. Schematic diagram of the dilatorquemeter. The parts of the armature are A_1—housing, A_2—rotation drive, A_3—rotation shaft. The parts of the torquemeter are T_1—body, T_2—moveable part, T_3—cross springs, T_4—capacitor plates, T_5—calibration coil. The dilatometer (which is drawn on a magnified scale compared with the torquemeter) fits in the cylindrical hole in the moveable part T_2 of the torquemeter. The parts of the dilatometer are D_1—sample (used as a lower capacitor plate), D_2—conical sample support, D_3—cell body, D_4—upper capacitor plate, D_5—spacer. D_3 and D_4 together constitute a guard ring for three-terminal capacitance measurement. The parts of the calibration drive are C_1—torquemeter, C_2—copper sample.

The dilatometer fits into the cylindrical hole in the moveable part T_2 of the torquemeter.

With this dilatorquemeter, simultaneous measurements can be made of relative length changes with a sensitivity of 2×10^{-11}, and of torques of the order of 0.1 dyn cm with a compliance of 2×10^{-7} rad/dyn cm. The quality of a de Haas–van Alphen torquemeter depends on the product of sensitivity and compliance, which for this instrument is 2×10^{-8}, and is comparable with that of more conventional torsion balances.

The magnetic field of the solenoid was accurately calibrated using a simple torquemeter C_1, which detects the neck orbit oscillations of an oriented copper crystal. This provides an accurate scale in $1/H$.

The combined oscillatory magnetostriction and torque method has been used to measure the uniaxial stress dependences of the Fermi surfaces of several other metals: Al, In, Mg, Zn,[14] Ga,[15] Pb,[16] and recently Cr,[17] W.[18] The group-VI transition

metals are among the hardest transition metals, and the oscillatory magnetostrictive length changes are typically two orders of magnitude smaller than in simple metals.[14] The torque amplitudes, are, however, comparable to those found in simple metals.

A major difficulty in the present experiments was to avoid any spurious length changes induced by the de Haas–van Alphen torque. Torque-induced length changes can be easily detected by measuring the amplitude $\Delta L/L$ of the oscillatory magnetostriction for magnetic field orientations near to a symmetry plane or direction of the lattice. If the frequency branch under consideration has a minimum or maximum at the chosen symmetry direction, and if Φ is the angle between the magnetic field and this symmetry direction, then (i) $\Delta L(\Phi)$ must be a symmetrical function of Φ if there are no torque-induced length changes; (ii) $\Delta L(\Phi)$ must be an antisymmetrical function of Φ if the observed length changes are entirely produced by torque effects. This technique proved to be very effective in testing various dilatometers, and showed that torque-induced effects can be minimized by using a relatively short sample whose length is approximately equal to its thickness, and by designing the dilatometer cell to have maximum rigidity. The single crystal used in this work was 7 mm long and 6 mm in diameter.

The oscillatory magnetostriction amplitude and the de Haas–van Alphen torque per unit volume τ, were measured at 1.2 K in fields up to 10.7 T. Since we wish to measure the response to tetragonal distortion, $\Delta L/L$ was measured along the [001] direction of the crystal lattice. The torque was measured about the [010] direction, which is also the axis about which the dilatorquemeter can be rotated. The angular dependence $d\ln A/d\Phi$ was determined from the measured de Haas–van Alphen frequency branches shown in Fig. 2. The labelling of the branches is the same as that used by Hoekstra and Stanford.[7] The frequencies shown in Fig. 2 are average values of the torque and magnetostriction frequencies, and are in excellent agreement with the measurements of Hoekstra and Stanford. The amplitude factor $\tau/(d\ln A/d\Phi)$, which for our experimental configuration is equal to the product of magnetization and magnetic field, is shown in Fig. 3 as a function of the magnetic field orientation, and $\Delta L/L$ is shown in Fig. 4. The torque amplitudes have cubic symmetry as all the measurements are made at zero stress. The length changes, however, have tetragonal symmetry relative to [001]. A comparison between Figs. 3 and 4 shows that for a given orbit both the torque amplitude factor and the oscillatory magnetostriction have similar angular dependences. The stress dependence $d\ln A/d\sigma$, where σ is a stress parallel to the [001] direction, calculated according to Eq. (1), is plotted in Fig. 5. Data for the octahedron orbit were taken over a reduced field range, and correspondingly the scatters in τ and $\Delta l/l$ were large, although the scatter in $(\Delta l/l)/\tau$ was less. For this reason, data for the octahedron have been omitted from Figs. 3 and 4, but its stress dependence is included in Fig. 5.

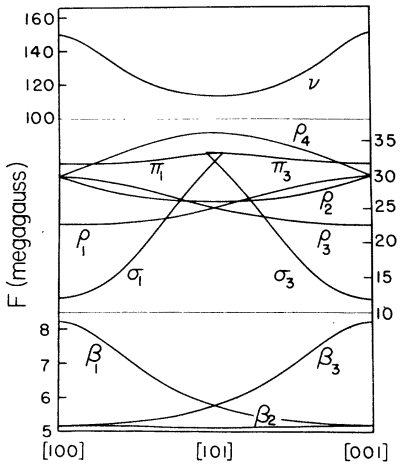

FIG. 2. de Haas–van Alphen frequencies in the (010) plane of molybdenum, determined in the course of the present experiments.

In general, the stress dependence is weakly dependent on orientation. The only exception is found for the octahedron centered at point H of the Brillouin zone. This is a large Fermi-surface sheet and, like the electron jack centered at Γ, there is only

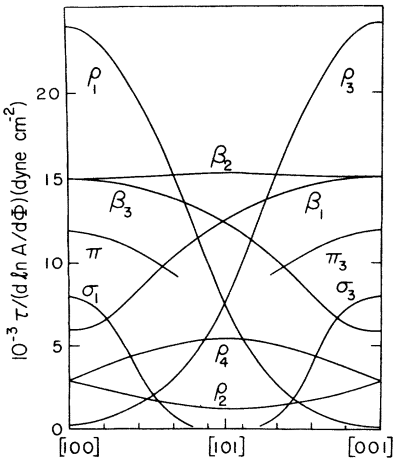

FIG. 3. Absolute amplitude of the de Haas–van Alphen torque per unit volume in molybdenum obtained by Fourier analysis of field sweeps in the range 4.6–10.7 T.

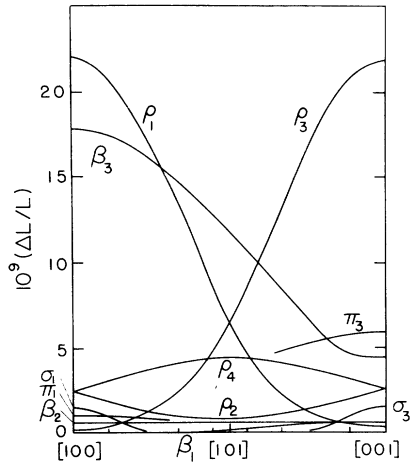

FIG. 4. Absolute amplitude of the oscillations of magnetostriction measured simultaneously with the torque data in Fig. 3.

one such sheet in the first Brillouin zone. Under a uniaxial stress it can only deform anisotropically, whereas a small pocket on a multiple sheet can exhibit an isotropic deformation which is associated with the transfer of electrons or holes to similar pockets that are inequivalent under the applied stress.

In view of the almost isotropic stress dependence observed for most of the Fermi surface of molybdenum, we shall, in Secs. III–V, analyze the experimental stress dependences for magnetic fields only in the [001] and [100] directions; that is, parallel and perpendicular to the stress. These results are summarized in Table I.

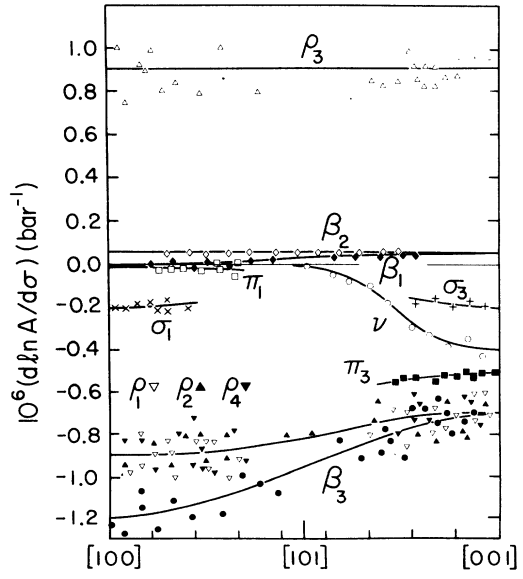

FIG. 5. Uniaxial stress dependence of extremal cross sections of the Fermi surface of molybdenum as a function of field orientation in the (010) plane. The nomenclature is that of Hoekstra and Stanford: β—lenses, σ—necks, π—balls, ρ—ellipsoids, ν—octahedron.

From the stress derivatives $d\ln A/d\sigma$ given in Table I the hydrostatic pressure dependence $d\ln A/dP$ can be calculated using the relation

$$\frac{d\ln A}{dP} = -\sum_i \frac{d\ln A}{d\sigma_i}, \tag{2}$$

where σ_i $(i = x, y, z)$ represents uniaxial stresses along the [100], [010], and [001] directions. The pressure dependences in Table II obtained in this way for the lenses and the ellipsoids are in good agreement with the direct hydrostatic pressure measurements of Svechkarev and Pluzhnikov.[11] It has been suggested by Griessen and Sorbello[14] in the context of similar investigations of the Fermi surfaces of simple metals that $(1/m^*)(dA/d\ln\Omega)$ has approximately the same value for corresponding orbits in different metals. It is therefore interesting to compare our volume derivatives for molybdenum with estimates obtained by scaling the pressure data of Schirber[19] in tungsten. The comparison in Table II shows good agreement between the two. The uniaxial strain dependences of the Fermi surface of chromium[20] and tungsten are also found to scale in a similar way, suggesting that this scaling property can be applied to d-band metals also.

In Table III the stress dependences are compared with values measured by Posternak *et al.*[10] for the smallest cross section of the lenses. The stress dependences have also been calculated from strain dependences determined by measuring simultaneously the oscillations of sound velocity and de Haas–van Alphen torque.[21] The results, also in Table III, are not in disagreement with the magnetostriction and torque data when allowance is made for the large experimental uncertainties associated with this technique.

III. STRAIN RESPONSES OF FERMI SURFACE

Calculations based on phase-shift parametrization have proved very successful in analyzing and correlating Fermi surface anisotropies with Fermi velocity anisotropies,[22] scattering of conduction electrons by phonons and impurities,[23] and conduction-electron spin relaxation.[24] In this approach, phase shifts at the Fermi energy of the metal are deduced by fitting the cross-sectional areas of the Fermi surface as deduced in de Haas–van Alphen experiments. In such an analysis the Fermi energy E_F enters as a parameter whose value cannot be determined from the fit to the data.[25] In practice, E_F is conveniently taken from the results of

TABLE I. Experimental stress derivatives of extremal cross sectional areas of the Fermi surface of molybdenum.

Orbit	A (a.u.)	i	$\frac{d\ln A}{d\sigma_i}$ (units of 10^{-6} bar^{-1})
σ neck orbit $\perp$ [001]	0.0314	x	−0.20(5)
		y	−0.20(5)
		z	−0.20(5)
π ball orbit $\perp$ [001]	0.0846	x	0.00(4)
		y	0.00(4)
		z	−0.50(5)
β lens circle $\perp$ [001]	0.0219	x	0.00(5)
		y	0.00(5)
		z	−0.7(2)
β lens along [001] orbit $\perp$ [010]	0.0138	x	0.05(1)
		y	0.05(1)
		z	−1.2(2)
ν octahedron orbit $\perp$ [001]	0.402	x	0.00(5)
		y	0.00(5)
		z	−0.40(15)
ρ ellipsoid at $(1,1,0)\pi/a$ orbit $\perp$ [001]	0.0607	x	−0.90(15)
		y	−0.90(15)
		z	+0.90(10)
ρ ellipsoid at $(1,1,0)\pi/a$ orbit $\perp$ [100]	0.0797	x	+0.90(25)
		y	−0.90(20)
		z	−0.70(20)

a first-principles band-structure calculation. Once the value of E_F has been assigned, the corresponding relativistic phase shifts $\eta_{l,j}(E_F)$ can be deduced. In this section we show how the phase-shift method can be extended to determine the deformation of the Fermi surface of a cubic metal (in this case bcc molybdenum) produced by arbitrary strains.

To introduce our notation for lattice deformation, consider unit vectors $\hat{x}$, $\hat{y}$, and $\hat{z}$, parallel to the edges of the conventional unit cell. The basis vectors of the direct lattice can be written in the form $\vec{\mathbf{x}} = a\hat{x}$. Under a uniaxial elongation the basis vectors take the form

$$\vec{\mathbf{x}}' = a\hat{x}(1+\epsilon_x). \tag{3}$$

The strains ϵ_i $(i = x,y,z)$ are accompanied by a volume change, and for this reason are not the most convenient way to represent our results. Instead we introduce three volume-conserving tetragonal shears γ_i whose associated strains are

$$\epsilon_x = \gamma_x, \quad \epsilon_y = \epsilon_z = -\tfrac{1}{2}\gamma_x, \tag{4}$$

and express the hydrostatic strain by the dilation of the lattice

$$\Delta\Omega/\Omega = \epsilon_x + \epsilon_y + \epsilon_z, \tag{5}$$

where Ω is the volume of the conventional unit cell. The three tetragonal shears are not independent—their sum is, of course, zero.

In order to describe completely the state of strain of a cubic metal, the elongations ϵ_i must be complemented by angular shears ϵ_{ij} which represent changes in the angles between the basis vectors of the lattice. If, for example, the lattice is subjected to an angular shear about the z axis the basis vectors of the strained lattice can be written

$$\vec{\mathbf{x}}' = a(\hat{x} + \epsilon_{xy}\hat{y}), \quad \vec{\mathbf{y}}' = a(\hat{y} + \epsilon_{yx}\hat{x}), \tag{6}$$

where ϵ_{xy} is the angle (in radians) through which the x axis is rotated towards the direction y. Our results will be expressed in terms of the more usual angular shear components

$$\gamma_{xy} = \epsilon_{xy} + \epsilon_{yx}. \tag{7}$$

Thus, a positive angular shear γ_{ij} corresponds to a reduction in the angle between the i and j axes of the real space lattice.

In the KKR method of band-structure calculation, the energy bands are determined by the implicit equation

$$\lambda(\vec{\mathbf{k}}, E, \eta_{l,j}, \epsilon) = 0, \tag{8}$$

where λ is the eigenvalue of the set of linear equa-

TABLE II. Hydrostatic pressure derivatives for molybdenum determined from (a) uniaxial stress data; (b) direct measurements by Svechkarev and Pluzhnikov (Ref. 11); (c) scaled from tungsten (Ref. 19) according to the expression

$$\left.\frac{d\ln A}{dp}\right|_{\mathrm{Mo}} = \frac{\kappa_{\mathrm{Mo}}}{\kappa_{\mathrm{W}}}\frac{A_{\mathrm{W}}}{A_{\mathrm{Mo}}}\frac{M^*_{\mathrm{Mo}}}{m^*_{\mathrm{W}}}\left.\frac{d\ln A}{dp}\right|_{\mathrm{W}},$$

where p is pressure and κ is compressibility. For lack of reliable band mass data for molybdenum and tungsten, equal cyclotron masses m^* were assumed. The compressibilities were taken from Ref. 29.

Orbit	A (a.u.)	$\frac{d\ln A}{dp}$ (a)	(b)	(c)
σ neck	0.0314	0.6(1)	···	0.81
π ball	0.0846	0.50(12)	···	0.58
β lens circle	0.0219	0.6(2)	···	···
β lens	0.0138	1.1(2)	1.47(15)	···
ν octahedron	0.402	0.4(2)	···	0.396
ρ ellipsoid $\perp$ [001]	0.0607	0.9(3)	0.9(1)	0.93
ρ ellipsoid $\perp$ [100]	0.0797	0.7(4)	···	···

tions

$$\sum_{l'm'} \mathcal{K}_{lml'm'} V_{l'm'} = \lambda V_{lm}. \tag{9}$$

The KKR matrix $\mathcal{K}_{lml'm'}$ depends parametrically on the energy E, the phase shifts $\eta_{l,j}(E)$, and the strain components ϵ. It is with this last dependence that we shall be especially concerned in the present paper.

The shape of the Fermi surface in the presence of an arbitrary strain can be determined by locating the wave vectors $\vec{k}$ that satisfy the equation

$$\lambda(\vec{k}, E_F, \eta_{l,j}, \epsilon) = 0, \tag{10}$$

where E_F and $\eta_{l,j}$ are in general functions of the strain ϵ. Our purpose is to determine directly the strain derivatives of the Fermi wave vector locally on the Fermi surface. This can be done by calculating analytically the appropriate derivative of the KKR matrix.

TABLE III. Comparison of stress derivatives for lenses in molybdenum obtained by different experimental methods: (a) present work; (b) low-field measurements of Posternak *et al.* (Ref. 10); (c) calculated from the strain derivative data (Ref. 21).

Orbit	i	$\frac{d\ln A}{d\sigma_i}$ (units of 10^{-6} bar^{-1}) (a)	(b)	(c)
β lens along [001]	x	0.05(1)	−0.1(2)	0.10(15)
Orbit $\perp$ [010]	y	0.06(1)	−0.2(2)	0.10(15)
A = 0.0138 a.u.	z	−1.2(2)	−1.1(3)	−1.30(15)

The variation in λ corresponding to an infinitesimal variation of a single parameter q is given by[26]

$$\left(\frac{\partial\lambda}{\partial q}\right)_{q'} = \sum_{lm,l'm'} (V^0_{lm})^{-1}\left(\frac{\partial\mathcal{K}_{lml'm'}}{\partial q}\right)_{q'} V^0_{l'm'}, \tag{11}$$

where V^0 is the zero eigenvector of the KKR matrix, and $\partial\mathcal{K}/\partial q$ is the matrix whose elements are the partial derivatives of $\mathcal{K}$ with respect to q. In order to remain on the surface $\lambda = 0$ [Eq. (10)], the variation in q must be accompanied by a variation in $\vec{k}_F$ whose component normal to the surface is given by

$$\frac{\partial k_F}{\partial q} = -\frac{\partial\lambda}{\partial q}(\nabla_{\vec{k}}\lambda)^{-1}. \tag{12}$$

For the purposes of the present work, partial derivatives of the relativistic KKR matrix were evaluated with respect to the Fermi energy parameter E_F, the phase shifts $\eta_{l,j}$, uniaxial elongations ϵ_i, and angular shears ϵ_{ij}. The calculation of the derivatives of the KKR structure constants for a cubic lattice subject to homogeneous strain will be described in detail elsewhere.[27]

The accuracy of the derivatives was verified in various ways. The energy and phase-shift dependences were checked by comparison with direct calculations in which small changes were made in the relevant parameters. The hydrostatic strain response was similarly checked by direct calculations with slightly different lattice parameters. The tetragonal- and angular-shear responses were checked by comparing with an augmented-plane-wave calculation for a strained lattice. In each case excellent agreement was obtained (typically 0.1%).

It is straightforward to determine the dependence of the cross-sectional area of an orbit on the parameter q by integrating around the orbit the projection of the normal displacement in the plane of the orbit. The result is

$$\left(\frac{\partial A}{\partial q}\right)_{q'} = \int_0^{2\pi} d\psi\, |k_\perp| \left(\frac{\partial\lambda}{\partial q}\right)_{q'} (\hat{k}_\perp \cdot \nabla_{\vec{k}}\lambda)^{-1}, \tag{13}$$

where $\vec{k}_\perp$ is the vector from the center to the perimeter of the orbit in the plane normal to the magnetic field, and ψ is the azimuthal angle. The dependences of the areas of extremal orbits on the various parameters were calculated by numerical integration of Eq. (13). The accuracy of the integration technique was checked by making a nearly-free-electron test in a body-centered-cubic lattice. The Fermi energy was chosen to be such that lens-like pockets of electrons are formed in the second

zone about the symmetry point N. In the usual form of the KKR equations, the structure factors are singular on the free-electron sphere. To avoid this difficulty, a very weak lattice potential was assumed in our calculation. When allowance is made for this, excellent agreement is found with the results of a direct free-electron calculation.

The starting point of our strain response calculations is the parametrization of the Fermi surface of molybdenum by Ketterson, Koelling, Shaw, and Windmiller.[8] In order to obtain full agreement with the experimental Fermi surface areas, they found it necessary to include parameters that represent departures from spherical symmetry of the potential within the muffin-tin sphere. In the present work we have neglected all terms that arise from nonspherical components of the potential. Such an approximation greatly simplifies the analysis, and appears justifiable because we are primarily concerned with derivatives of Fermi-surface areas with respect to geometrical deformations of the lattice. Such derivatives are known with experimental accuracies of no better than about 20%.

The five relativistic phase shifts of the spherical muffin-tin potential in molybdenum were taken from the parameters of the best fit to the Fermi surface data by Ketterson *et al.* Because the phase shifts of their best spherical fit to the Fermi surface were unavailable, we estimated $\eta_{2,5/2}$ as an appropriately weighted average of $\eta_{\Gamma_{7,2,5/2}^{+}}$ and $\eta_{\Gamma_{8,2,5/2}^{+}}$. Following Ketterson *et al.*, the equilibrium lattice parameter was assigned the room-temperature value $a_0 = 5.9468$ a.u., and the Fermi energy parameter was taken to be $E_F = 0.754$ Ry. This leads to the following set of phase shifts (radians):

$$\eta_{0,1/2} = -0.742\,13,$$
$$\eta_{1,1/2} = -0.315\,80, \quad \eta_{1,3/2} = -0.300\,73, \tag{14}$$
$$\eta_{2,3/2} = -1.1072, \quad \eta_{2,5/2} = -1.2922.$$

The phase-shift difference

$$\Delta_l \equiv \eta_{l,l+1/2} - \eta_{l,l-1/2} \tag{15}$$

measures the strength of the spin-orbit interaction for given l in the metal. The fit to the Fermi-surface data shows that in molybdenum p-wave spin-orbit interaction is weak, whereas d-wave spin-orbit interaction is quite strong. However, it is important to note that the best fit to the Fermi-surface areas is such that small variations of the phase-shift parameters may still yield a model surface that is consistent with the area data.

Molybdenum is an interesting subject for strain studies because the various extremal orbits on the Fermi surface pass through regions of widely different symmetry character. We may therefore expect that the strain responses of the various orbits will yield information about different partial-wave components of the lattice potential. The varying symmetry character from orbit to orbit is reflected in the phase-shift derivatives of orbital areas calculated from our model Fermi surface, which are given in Table IV. It will be seen that the neck, ball, and lens orbits are predominantly d-like, and that the lens orbits are strongly influenced by d-wave spin-orbit interaction. The octahedron orbit ν_1 is p- and d-like. The ellipsoid orbits are predominantly p-like, and are the only orbits having significant admixture of s-wave character.

The response of extremal cross-sectional areas of the Fermi surface to elongations ϵ_i in the x, y, and z directions was calculated by application of Eqs. (11) and (13). The results were combined to form a tetragonal-shear component and a dilation component as in Eqs. (4) and (5). To see why it is convenient to express our results in this form let us show that a typical scalar parameter, the phase shift η_l, is unchanged to first order when a cubic lattice is subjected to a volume-conserving elongational shear γ. The strain dependence of η_l can be written

$$\frac{\partial \eta_l}{\partial \gamma} = \sum_i \frac{\partial \eta_l}{\partial \epsilon_i} \frac{\partial \epsilon_i}{\partial \gamma}. \tag{16}$$

Because η_l is a scalar, the three coefficients

TABLE IV. Dependence of areas of some extremal orbits on the Fermi surface of molybdenum on dilation and on phase shifts in angular momentum representation (in radians).

Orbit	A (a.u.)	$\left(\frac{\partial \ln A}{\partial \ln \Omega}\right)_{E_F,\eta}$	$\left(\frac{\partial \ln A}{\partial \eta_0}\right)_{E_F,\Omega}$	$\left(\frac{\partial \ln A}{\partial \eta_{1,1/2}}\right)_{E_F,\Omega}$	$\left(\frac{\partial \ln A}{\partial \eta_{1,3/2}}\right)_{E_F,\Omega}$	$\left(\frac{\partial \ln A}{\partial \eta_{2,3/2}}\right)_{E_F,\Omega}$	$\left(\frac{\partial \ln A}{\partial \eta_{2,5/2}}\right)_{E_F,\Omega}$
σ neck	0.0314	5.2585	0.0157	0.0645	0.7157	3.7140	2.9165
π ball	0.0846	3.7068	0.0366	0.5765	1.1028	1.6039	2.4818
β lens circle	0.0219	8.8768	0.0128	0.3838	0.3697	1.3826	9.4299
β lens $\perp$ [010]	0.0138	9.3512	0.0018	0.1735	0.2504	2.4271	9.0816
ν octahedron	0.402	−2.1187	−0.0111	−0.4998	−0.3895	−0.6803	−0.5160
ρ ellipsoid $\perp$ [001]	0.0607	−8.1515	−0.7884	−3.4929	−6.7833	−0.5516	−0.6137
Ellipsoid $\perp$ [100]	0.0797	−7.8670	−0.2715	−3.7424	−7.1362	−0.5319	−0.6189

$\partial\eta_l/\partial\epsilon_i$ must be equal in a cubic lattice. So the strain dependence of η_l can be written

$$\frac{\partial\eta_l}{\partial\gamma}=\frac{\partial\eta_l}{\partial\epsilon}\sum_i\frac{\partial\epsilon_i}{\partial\gamma}\,, \tag{17}$$

which vanishes [Eq. (4)] for a volume-conserving elongational shear. Therefore, the first-order response of the Fermi surface of a cubic metal to such a shear depends on the perturbation of the electronic band structure by the lattice deformation at constant values of the scalar parameters η_l and E_F. This means that the tetragonal-shear response can be calculated directly from a phase-shift fit to the Fermi-surface data, and no additional parameters are involved. A more general treatment of shear dependence of η_l and E_F, including angular shear and the extension to noncubic metals, has recently been presented by Gray and Gray.[28]

A comparison between the tetragonal-shear response of extremal orbits calculated from our model [Eq. (14)] and the experimental data is presented in Table V. Complete agreement with the data is not achieved, but the discrepancy is generally smaller than twice the uncertainty in the experimental data. The principal exception is for the neck orbit (σ), where no tetragonal-shear response is observed experimentally, but where the calculation predicts a sizable effect. The calculated tetragonal-shear response of the Fermi surface of molybdenum in the {100} planes is illustrated in Fig. 6. In order to investigate the remaining discrepancy one would like to carry out an iterative calculation to fit the phase shifts to both the area and the tetragonal-shear data. Unfortunately, such a calculation is greatly complicated by the fact that

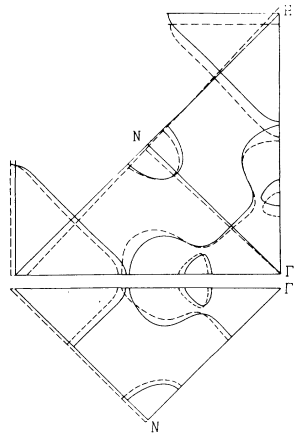

FIG. 6. Tetragonal shear response of the Fermi surface of molybdenum (a) in the (100) plane containing the shear axis, (b) in the plane perpendicular to the shear axis, for a tetragonal shear $\gamma_z=0.04$. The direction of the shear is vertical.

TABLE V. Tetragonal shear dependence of areas of some extremal orbits on the Fermi surface of molybdenum.

Orbit	i	A (a.u.)	$\frac{d\ln A}{d\gamma_i}$ Expt.	Calc.
σ neck orbit $\perp$[001]	x	0.0314	0.0(3)	−1.32
	y		0.0(3)	−1.32
	z		0.0(6)	2.65
π ball orbit $\perp$[001]	x	0.0846	0.79(15)	0.50
	y		0.79(15)	0.50
	z		−1.58(30)	−1.00
β lens circle $\perp$[001]	x	0.0219	0.95(35)	1.44
	y		0.95(35)	1.44
	z		−1.89(70)	−2.88
Lens along [001]	x	0.0138	1.98(35)	1.75
orbit $\perp$[010]	y		2.00(35)	2.99
	z		−3.98(70)	−4.74
ν octahedron orbit $\perp$[001]	x	0.402	0.63(30)	1.22
	y		0.63(30)	1.22
	z		−1.26(60)	−2.44
ρ ellipsoid at $(1,1,0)\pi/a$	x	0.0607	−2.83(45)	−4.63
orbit $\perp$[001]	y		−2.83(45)	−4.63
	z		5.67(90)	9.27
Ellipsoid at $(1,1,0)\pi/a$	x	0.0797	−2.20(60)	−2.27
orbit $\perp$[100]	y		−3.20(60)	−5.61
	z		5.40(120)	7.88

TABLE VI. Isotropic dilation dependence of areas of some extremal orbits on the Fermi surface of molybdenum.[a]

Orbit	A (a.u.)	$\frac{d\ln A}{d\ln\Omega}$ Uniaxial	Pressure	Calc.
σ neck	0.0314	−1.6(3)	···	−1.77
π ball	0.0846	−1.3(3)	···	−1.07
β lens circle	0.0219	−1.6(5)	···	−2.50
lens $\perp$[010]	0.0138	−2.9(6)	−3.8(4)	−2.65
ν octahedron	0.402	−1.1(5)	···	−0.59
ρ ellipsoid $\perp$[001]	0.0607	−2.4(8)	−2.4(4)	−2.40

[a] The experimental results were calculated taking the isothermal compressibility to be 0.38×10^{-6} bar^{-1}. The calculated volume dependence is determined from the following set of parameters (radians):

$$\frac{d\eta_{0,1/2}}{d\ln\Omega}=-1.1910,\quad \frac{d\eta_{1,1/2}}{d\ln\Omega}=\frac{d\eta_{1,3/2}}{d\ln\Omega}=-0.3525,$$

$$\frac{d\eta_{2,3/2}}{d\ln\Omega}=-1.0107,\quad \frac{d\eta_{2,5/2}}{d\ln\Omega}=-1.0324.$$

Phase shifts correspond to $E_F=0.754$ Ry.

the centers of the neck, lens circle, and ball orbits are not determined by symmetry. They therefore move as the phase shifts are varied, and must be recalculated at each iteration. In view of the amount of computer time involved, we did not attempt a systematic iterative calculation.

The dilation response of the Fermi surface of molybdenum calculated from the pressure derivative data of Table I, using compressibility data of Featherston and Neighbours,[29] is given in Table VI. In our phase-shift model of the Fermi surface, the dilation component of the strain response depends not only on the phase-shifts of the unperturbed lattice, but also on the dilation dependence of the phase shifts. This can be brought about both by the changing overlap between the crystal potentials on nearby lattice sites as the lattice is compressed, and also by dilation dependence of the Fermi energy, of which the phase shifts are a function. In discussing the effects of lattice dilation, variations of the Fermi energy must be carefully distinguished from variations of the Fermi energy parameter. The Fermi energy parameter is a free parameter in a phase-shift fit to Fermi-surface data; that is, its value can be assigned arbitrarily provided that the phase shifts are chosen accordingly.[25] In particular, one is free to take the dilation dependence of the Fermi energy parameter to be zero.

The experimental results for molybdenum have been analyzed by making a least-squares fit to the dilation data in the form

$$\frac{d\ln A}{d\ln\Omega} = \left(\frac{\partial \ln A}{\partial \ln\Omega}\right)_{\eta, E_F} + \left(\frac{\partial \ln A}{\partial E_F}\right)_{\eta,\Omega} \frac{dE_F}{d\ln\Omega} + \sum_{lj} \left(\frac{\partial \ln A}{\partial \eta_{l,j}}\right)_{\eta, E_F} \frac{d\eta_{l,j}}{d\ln\Omega}. \tag{18}$$

The form of the dilation dependence of the (100) plane of the Fermi surface of molybdenum is illustrated in Fig. 7. The coefficients $(\partial \ln A/\partial \ln\Omega)_{\eta,E_F}$ and $(\partial \ln A/\partial \eta_{l,j})_{\eta,E_F}$ were calculated from the phase-shift model, and are given in Table IV. As explained above, we have set the parameters $dE_F/d\ln\Omega$ equal to zero: any other choice is admissible but yields different values for $d\eta_{l,j}/d\ln\Omega$. The result of the least-squares fit to the experimental data is presented in Table VI. It will be seen that a generally satisfactory fit to the data is achieved, which supports the adequacy of our model. However, for reasons we do not understand, the predicted strain dependence of the octahedron orbit is low, with the consequence that the calculated pressure derivatives of electron and hole volumes do not show exact compensation. The best values of the total derivatives

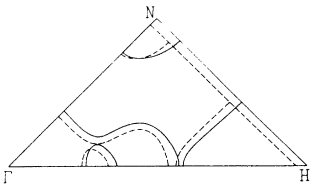

FIG. 7. Calculated deformation of the Fermi surface of molybdenum in the (100) plane for a dilation $\Delta\Omega/\Omega = 0.10$.

obtained from the fit to the data are

$$\frac{d\eta_{0,1/2}}{d\ln\Omega} = -1.19 \pm 1.25 \text{ rad},$$

$$\frac{d\eta_{1,1/2}}{d\ln\Omega} = -0.35 \pm 0.09 \text{ rad},$$

$$\frac{d\eta_{1,3/2}}{d\ln\Omega} = -0.35 \pm 0.09 \text{ rad}, \tag{19}$$

$$\frac{d\eta_{2,3/2}}{d\ln\Omega} = -1.01 \pm 0.05 \text{ rad},$$

$$\frac{d\eta_{2,5/2}}{d\ln\Omega} = -1.03 \pm 0.02 \text{ rad}.$$

These estimates all correspond to $E_F = 0.754$ Ry. Whilst no direct calculations have been carried out to determine the volume derivatives of the phase shifts from a crystal potential, the negative signs are consistent with the view that the crystal potential becomes weaker as the lattice expands. Unfortunately the small number of orbits included in the analysis made it necessary to constrain the volume dependence of the p-wave spin-orbit parameter

$$\Delta_1 \equiv \eta_{1,3/2} - \eta_{1,1/2} \tag{20}$$

to be equal to zero. However, the validity of this assumption is supported by our result that the volume dependence of the d-wave spin-orbit parameter

$$\Delta_2 \equiv \eta_{2,5/2} - \eta_{2,3/2} \tag{21}$$

does not differ significantly from zero. That the spin-orbit phase shifts should be essentially independent of volume is suggested by the following physical considerations. The spin-orbit coupling is determined by the potential gradient close to the nucleus. Although the changing overlap associated with lattice dilation will modify the potential acting on the electron, it is unlikely to affect the potential *gradient* within the core, and hence is not expected to lead to a significant variation in the spin-orbit phase shifts. The dilation dependence of the spin-orbit energy is expected to be dominated by the varying normalization of

the conduction-electron wave functions within the dilated unit cell.[30]

IV. RESPONSE OF FERMI SURFACE TO ANGULAR SHEAR

In order to describe completely the state of deformation of a cubic metal, strains ϵ_i which represent extensions along the cube axes of the conventional unit cell, must be complemented by strains γ_{ij} which represent changes in the angles between the basis vectors of the lattice. The KKR matrix depends on the vectors of the real lattice and on those of the reciprocal lattice, both of which are changed by angular shear, and therefore the KKR matrix depends parametrically on γ_{ij}. It follows that derivatives of the Fermi wave vector with respect to a volume conserving angular shear can be calculated in the manner of Sec. III. By an argument similar to that developed above for tetragonal shear it can be shown that, in first order, the distortions of the Fermi surface of a cubic metal subjected to angular shear depend only on the geometry of the deformation.[28] Therefore, our phase shift model fully determines the angular-shear dependence of the Fermi surface of a cubic metal, without involving any additional parameters.

In a cubic metal subjected to angular shear about the [001] axis, states which belong to one-dimensional irreducible representations and which lie in the (100) and (010) planes through the center of the Brillouin zone are unaffected by the strain. In general, however, the magnitude of the Fermi wave vector in an arbitrary direction depends on angular shear. Nevertheless, by taking into account both the orbital symmetry and also the symmetry of the strain, it can be shown that the areas of many extremal orbits of high symmetry are unchanged to first order in the angular shear. The area derivative $d\ln A/d\gamma_{xy}$ vanishes for reasons of symmetry for any extremal orbit: (a) whose center lies on the [001] axis, and whose normal lies in the (100) plane; (b) whose center lies at a general point on the [100] axis, and whose normal lies in the (100) or (010) plane; (c) whose center lies at a general point in the (010) plane, and whose normal lies in the (010) plane. In each of these conditions, references to [100] or (100) can, of course, be replaced by [010] or (010), respectively.

Applying these conditions to molybdenum, it will be seen that the areas of the principal neck, ball, and lens orbits, show no angular shear dependence, in accordance with (a) and (b). On the octahedra, all of the [100] orbits, and four of the six [110] orbits, are independent of angular shear in accordance with (a). The 12 ellipsoids split into two inequivalent sets: four ellipsoids centered in the plane through Γ perpendicular to the axis of shear, and eight centered elsewhere. The ellipsoids of the first set show strong dependence on angular shear. On ellipsoids of the second set, the angular-shear dependence of all principal (and certain nonprincipal) extremal orbits vanishes in accordance with the symmetry considerations above. Other extremal orbits on these ellipsoids prove to be relatively weakly dependent on angular shear: for example, we find that the angular-shear response of the [111] orbits is in the ratio 4.2 to 1 between the two sets of ellipsoids.

The angular-shear dependences of the areas of some representative orbits on the Fermi surface of molybdenum are shown in Table VII, and the form of the angular-shear response in the (001) plane perpendicular to the shear axis is shown in Fig. 8. The response is zero in the {001} planes containing the shear axis for reasons of symmetry. Our calculations predict a significantly anisotropic angular-shear dependence on the ellipsoid. Measurements of the angular-shear response of the Fermi surface of molybdenum by observing, for example, the oscillatory velocity of transverse sound waves, would provide a useful test of the model on which our calculations are based. Because, however, the areas of few of the principal orbits in molybdenum are sensitive to angular shear, and because orbits on the ellipsoids show

TABLE VII. Angular-shear dependence on some extremal orbits on the Fermi surface of molybdenum. γ_{ij} is measured in radians.

Orbit	ij	A (a.u.)	$\frac{d\ln A}{d\gamma_{ij}}$
σ neck	xy, yz, zx	0.0314	0
π ball	xy, yz, zx	0.0846	0
β lens	xy, yz, zx	0.0219	0
lens along [001] orbit $\perp$ [010]	xy, yz, zx	0.0138	0
ν octahedron at $(2,0,0)\pi/a$ orbit $\perp$ [100]	xy, yz, zx	0.402	0
ν octahedron at $(2,0,0)\pi/a$ orbit $\perp$ [110]	xy	0.302	1.83
	yz, zx		0
ν octahedron at $(2,0.0)\pi/a$ orbit $\perp$ [111]	xy, yz, zx	0.276	0.67
ρ ellipsoid at $(1,1,0)\pi/a$ orbit $\perp$ [001]	xy	0.0607	−3.55
	yz, zx		0
ρ ellipsoid at $(1,1,0)\pi/a$ orbit $\perp$ [110]	xy	0.0701	−4.93
	yz, zx		0
ρ ellipsoid at $(1,1,0)\pi/a$ orbit $\perp$ [1$\bar{1}$0]	xy	0.0971	−6.69
	yz, zx		0

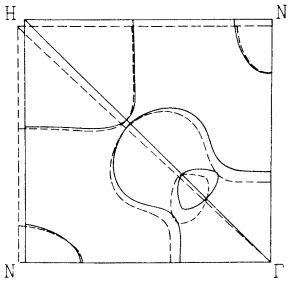

FIG. 8. Angular shear response of the Fermi surface of molybdenum in the (001) plane perpendicular to the shear axis. The curve corresponds to an angular shear γ_{xy} of 3 deg.

little variation of symmetry character (they have mainly p character everywhere), measurements of angular-shear dependence of orbital areas yield rather incomplete information about the global angular-shear response of the Fermi surface. We anticipate that only by means of a reliable calculation, supplemented by strain data, will it be possible to determine the angular-shear deformation parameter at each point of the Fermi surface.

V. DISCUSSION AND CONCLUSIONS

In this paper we have presented the first detailed investigation of the response of a Fermi surface to homogeneous uniaxial deformation of the lattice. Even in molybdenum, which is one of the hardest transition metals, the combined oscillatory magnetostriction and de Haas–van Alphen torque method proved to be very effective. Although the relative length changes associated with the oscillatory magnetostriction are in general much smaller than 10^{-8}, the use of a capacitor dilatorquemeter made it possible to determine accurately the stress dependence of extremal cross sections of the Fermi surface. In the case of the lenses and the ellipsoids, where our results can be compared with direct hydrostatic pressure measurements, good agreement is found.

From our uniaxial stress data we determined the tetragonal and hydrostatic strain dependences of various orbits of high symmetry on the Fermi surface. The strain derivative $d\ln A/d\epsilon$ represents an average about an orbit, and in order to deduce the strain dependence at each point on the Fermi surface it is essential to construct a model band structure whose parameters can be adjusted to fit the experimental data. The model band structure must represent as closely as possible the physical effects associated with lattice distortion in order to make the most efficient use of the rather small number of independent pieces of information that are contained in the data.

Our calculation is based on the usual muffin-tin approximation, where the potential is taken to be spherically symmetric within a sphere centered on each lattice site, and constant elsewhere. Ketterson *et al.*[8] found that this approximation leads to small but significant errors in the cross-sectional areas of the computed Fermi surface. However, introducing a cubic component in the muffin-tin potential involves two more parameters, one being an additional phase shift associated with the crystal-field splitting of the $\Gamma_7^+, 2, 5/2$ and $\Gamma_8^+, 2, 5/2$ representations, and the other being the coupling between the $\Gamma_8^+, 2, 3/2$ and $\Gamma_8^+, 2, 5/2$ states caused by the cubic field. As four adjustable parameters have already been introduced in the spherical approximation to fit the hydrostatic strain data, (Table VI), it is clear from an examination of the data that sufficient additional information is not available to determine parameters associated with the volume dependence of the cubic crystal field. Presumably such effects are to some extent folded into the volume dependences of the spherical phase shifts determined in Sec. III.

Applying a tetragonal shear further lowers the symmetry of the crystal field, splitting apart states that are degenerate in an isotropically dilated crystal. To parametrize the tetragonal shear data, taking fully into account the tetragonal distortion of the crystal field, would require at least four additional parameters. The additional complexity of such a calculation will be justifiable only when new and substantially more accurate experimental data become available. It seems likely that the effects of a tetragonal distortion of the crystal field can be folded to some extent into the spherical phase shifts, so there is no reason to suppose that the best fit to the combined area and tetragonal-shear data should necessarily coincide with the best fit to the area data alone. However, we find reasonable agreement with the tetragonal-shear response of the Fermi surface by assuming spherical phase shifts that are derived from Fermi-surface area data alone. This suggests that strain-dependent tetragonal-shear distortions of the crystal field are not the principal factor in determining the tetragonal-shear response, and that it depends mainly on purely geometric effects of the distortion.

Angular shear leads to a pattern of distortion of the crystal field which largely removes the degeneracy of the d-like states. Again a full analysis would require that phase shifts be introduced which correspond to each of the irreducible representations of the distorted lattice, and in view of the limited information available, even in principle, from angular-shear measurements, it seems un-

likely that the additional parameters could be determined from oscillatory sound velocity data. The success of our spherical potential approach for tetragonal shear gives reason to hope that any corrections can be absorbed in the spherical phase shifts. In principle one might increase the information available from angular-shear measurements by examining orbits which lie out of the symmetry planes, but experimental and theoretical complications make it unlikely that such an approach will be undertaken in the near future.

It is interesting to note that, although the uniaxial stress derivatives of the third band monster orbits in aluminium[14] are approximately two orders of magnitude larger than those found in molybdenum, the scaled strain derivatives $(1/m^*) \times (dA/d\epsilon)$ are of comparable magnitude in the two metals.[31] This implies that strain derivatives scaled by the factor A/m^*, i.e., expressions $(1/m^*)(dA/d\epsilon)$, where ϵ is a homogeneous strain, are more significant quantities than $d\ln A/d\epsilon$. The physical significance of this observation is not understood.

In the case of simple models, such as the free-electron model or the pure d-band resonance model, $d\ln A/d\ln\Omega$ has a simple interpretation and is equal to $-\frac{2}{3}$. In these models, the deformation of the band structure can be described by scaling laws such as

$$A = (1/\Omega^{2/3}) f(E_F \Omega^{2/3}) \tag{22}$$

for free electrons, and

$$A = (1/\Omega^{2/3}) f((E_F - d_0)\Omega^{5/3}) \tag{23}$$

in Heine's resonance model,[32] in which d_0 corresponds approximately to the center of gravity of the pure d band whose width varies as $\Omega^{-5/3}$. The fact that the experimental $d\ln A/d\ln\Omega$ values are significantly different from $-\frac{2}{3}$ shows clearly that the strain dependence of the Fermi surface is inherently $\vec{k}$ dependent.

As the Fermi surface of molybdenum is very similar to that of paramagnetic chromium, we shall conclude by attempting to gain some qualitative information about the pressure dependence of itinerant antiferromagnetism in chromium from our knowledge of the strain dependence of the Fermi surface of molybdenum. The antiferromagnetism of chromium is due to a spin-density wave. According to a model proposed by Lomer,[33] the spin-density wave is stabilized by the occurrence of large parallel regions on the paramagnetic Fermi surface. In both chromium and molybdenum, a point on the electron jack can be brought into coincidence with a point on the hole octahedron by translation through a wave vector in the z direction

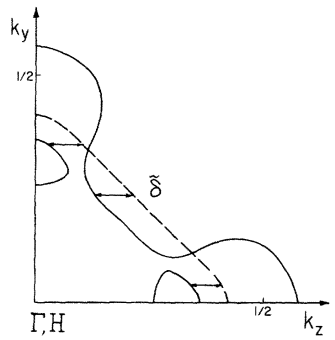

FIG. 9. Relationship between the form of the electron jack and the octahedron referred to a common center, and definition of $\tilde{\delta}(0,k_y)$. k_y, k_z are measured in units of $2\pi/a$.

$$\vec{\tilde{Q}}(k_x, k_y) = (2\pi/a)(0, 0, 1 \pm \tilde{\delta}(k_x, k_y)), \tag{24}$$

where $\tilde{\delta}(k_x, k_y)$ is only weakly dependent on the transverse wave vector (k_x, k_y) because these two sheets of the Fermi surface have almost the same shape. In Figs. 9 and 10 we show $\tilde{\delta}(0, k_y)$ as calculated from our model Fermi surface for molybdenum. Our results are very similar to those of Rath and Callaway.[34] The discontinuities are a consequence of the energy gaps that separate the lenses from the electron jack. Also in Fig. 10 we show the volume derivative $d\tilde{\delta}(0, k_y)/d\ln\Omega$. This derivative shows a marked anisotropy, which arises because the electron jack and the octahedron change their shapes in different ways under hydrostatic pressure. The volume derivative is positive everywhere, however, because the octahedron shrinks relative to the jack under hydrostatic pressure.

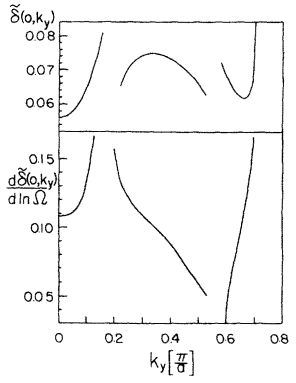

FIG. 10. Anisotropy of $\tilde{\delta}(0,k_y)$ calculated from the model Fermi surface based on the phase shifts of Eq. (14). We also show the volume derivative of $\tilde{\delta}$ obtained from the fitted volume dependence of the phase shifts given in Eq. (19).

The wave vector of the spin-density wave in chromium is usually expressed in the form

$$\vec{Q}=(2\pi/a)(0,0,1-\delta)\,, \tag{25}$$

where $\delta = 0.0481$. Griessen *et al.*[17] have made low-temperature measurements of the pressure derivative of δ and find it to be

$$\frac{d\ln\delta}{d\ln\Omega}=+0.33\pm0.27\,. \tag{26}$$

From the volume dependence of the Fermi surface of molybdenum (Fig. 10) we find

$$\frac{d\ln\delta}{d\ln\Omega}=+1.4\pm0.7\,. \tag{27}$$

A numerical discrepancy is to be expected because our calculation underestimates the volume dependence of the octahedra. The qualitative agreement between these estimates seems to support Lomer's suggestion that δ is simply related to a Fermi-surface average of $\bar{\delta}(k_x,k_y)$.

At higher temperatures, however, neutron-diffraction experiments[35] show that the pressure derivative of δ is negative and two orders of magnitude larger than at 0 K. As the pressure derivative of $\bar{\delta}(k_x,k_y)$ is not expected to be strongly temperature dependent, the probable explanation is that the relationship between $\bar{\delta}(k_x,k_y)$ and δ is temperature dependent. This conclusion is not surprising, for $\bar{\delta}(k_x,k_y)$ is a purely geometrical property of the Fermi surface, whereas δ is determined by minimizing the total energy in the antiferromagnetic state. In fact, it is not at present understood why the geometric Q calculated from a paramagnetic Fermi surface is in such good agreement with the antiferromagnetic Q at low temperature. No model proposed to date explains satisfactorily the observed temperature and pressure dependence of the wave vector of the spin-density wave.

In summary, we have shown that the relativistic KKR–spherical potential model derived from the shape of the Fermi surface of molybdenum, gives a satisfactory account of the response of the Fermi wave vector to homogeneous uniaxial strain. We believe that this model will prove to be a realistic starting point for analyzing related electronic properties such as the damping of acoustic waves in metals by interaction with the conduction electrons. An accurate description of strain effects at the Fermi energy is a necessary first step towards a better understanding of the stress dependence of the Fermi-surface properties of transition metals, such as the susceptibility and specific heat, as well as those properties, such as the cohesive energy and the elastic constants, which depend more generally on the way the electronic structure is perturbed by elastic strain.

ACKNOWLEDGMENTS

We wish to express our gratitude to Dr. N. A. W. Holzwarth for help in extending the KKR method to deformed lattices. We are also indebted to Professor E. Fawcett and Professor J. M. Perz, and to Dr. M. Posternak, for their interest in this work and for many helpful discussions. We would also like to thank W. Joss for his assistance in the early stages of this work, and D. Britton for the high-precision machining of the dilatorquemeter. The molybdenum crystal was generously supplied by Professor J. L. Olsen, and Dr. I. M. Templeton kindly gave us the oriented copper crystal used in field calibration. We are grateful to Dr. D. M. Gray for helpful comments on the manuscript.

---

*Work supported in part by the NRC of Canada.

†Present address: Natuurkundig Laboratorium der Vrije Universiteit, Amsterdam, The Netherlands.

‡Present address: Materials Physics Division, AERE Harwell, Didcot, Oxfordshire, England OX11 0RA.

[1]N. E. Alekseevskii, V. S. Egorov, G. E. Karstens, and B. N. Kazak, Sov. Phys. JETP 16, 519 (1963).

[2]E. Fawcett and W. A. Reed, Phys. Rev. 134, A723 (1964).

[3]C. K. Jones and J. A. Rayne, Phys. Lett. 8, 155 (1964).

[4]V. V. Boiko, V. A. Gasparov, and I. G. Gverdtsiteli, Zh. Eksp. Teor. Fiz. 56, 489 (1969) [Sov. Phys.–JETP 29, 267 (1969)].

[5]J. R. Cleveland and J. L. Stanford, Phys. Rev. B 4, 311 (1971).

[6]D. M. Sparlin and J. A. Marcus, Phys. Rev. 144, 848 (1966).

[7]J. A. Hoekstra and J. L. Stanford, Phys. Rev. B 8, 1416 (1973).

[8]J. B. Ketterson, D. D. Koelling, J. C. Shaw, and L. R. Windmiller, Phys. Rev. B 11, 1447 (1975).

[9]Y. Onodera and M. Okazaki, J. Phys. Soc. Jpn. 21, 1273 (1966).

[10]M. Posternak, W. B. Waeber, R. Griessen, W. Joss, W. van der Mark, and W. Wejgaard, J. Low. Temp. Phys. 21, 47 (1975).

[11]I. V. Svechkarev and V. B. Pluzhnikov, Phys. Status Solidi B 55, 315 (1973).

[12]A. B. Pippard, *The Dynamics of Conduction Electrons* (Gordon and Breach, New York, 1965), p. 110.

[13]B. S. Chandrasekhar, Phys. Lett. 6, 27 (1963).

[14]R. Griessen and R. S. Sorbello, Phys. Rev. B 6, 2198 (1972); R. Griessen and R. S. Sorbello, J. Low Temp. Phys. 16, 237 (1974).

[15]R. Griessen, H. Krugmann, and H. R. Ott, Phys. Rev. B 10, 1160 (1974).

[16]W. Joss, R. Mak, and R. Griessen (unpublished).
[17]R. Griessen, D. J. Stanley, and E. Fawcett (unpublished).
[18]D. J. Stanley, J. M. Perz, M. J. G. Lee, and R. Griessen, Can. J. Phys. 55, 344 (1977).
[19]J. E. Schirber, Phys. Lett. A 35, 194 (1971).
[20]E. Fawcett, R. Griessen, and D. J. Stanely (unpublished).
[21]R. Griessen and D. J. Stanley (unpublished).
[22]M. J. G. Lee, Phys. Rev. B 2, 250 (1970).
[23]P. T. Coleridge, N. A. W. Holzwarth, and M. J. G. Lee, Phys. Rev. B 10, 1213 (1974).
[24]N. A. W. Holzwarth and M. J. G. Lee (unpublished).
[25]M. J. G. Lee and V. Heine, Phys. Rev. B 5, 3839 (1972).
[26]P. O. Löwdin, J. Mol. Spectrosc. 13, 326 (1964).
[27]M. J. G. Lee and N. A. W. Holzwarth (unpublished).
[28]D. M. Gray and A. M. Gray, Phys. Rev. B 14, 669 (1976).
[29]F. H. Featherston and J. R. Neighbours, Phys. Rev. 130, 1324 (1963).
[30]D. Brust and L. Liu, Solid State Commun. 4, 193 (1966).
[31]R. Griessen, D. J. Stanley, E. Fawcett, M. Posternak, and W. Joss, Europhysics Conference Proceedings, Part I, Leuven, 1975 (unpublished).
[32]V. Heine, in *The Physics of Metals. I. Electrons*, edited by J. M. Ziman (Cambridge U.P., London, 1969), p. 1.
[33]W. M. Lomer, Proc. Phys. Soc. Lond. 80, 489 (1962).
[34]J. Rath and J. Callaway, Phys. Rev. B 8, 5398 (1973).
[35]H. Umebayashi, G. Shirane, B. C. Frazer, and W. B. Daniels, J. Phys. Soc. Jpn. 24, 368 (1968).